Mesoscale physical processes and the related impact on the summer nutrient fields and phytoplankton blooms in the western Gulf of Finland

JUSS PAVELSON

Marine Systems Institute
TALLINN UNIVERSITY OF TECHNOLOGY

Dissertation was accepted for the commencement of the degree of Doctor of Philosophy in Natural Sciences on June 21, 2005

Supervisor: Dr. Jaan Laanemets, Marine Systems Institute at Tallinn University of Technology

Opponents: Dr. Kai Myrberg, Finnish Institute of Marine Research

Dr. Tiina Nõges, Institute of Agricultural and Environmental Sciences at the Estonian Agricultural University

Commencement: September 15, 2005 at the Institute of Cybernetics at Tallinn University of Technology, Akadeemia tee 21, Tallinn, Estonia

Declaration: Hereby I declare that this doctoral thesis, my original investigation and achievement, submitted for the doctoral degree at Tallinn University of Technology has not been submitted for any degree or examination.

Juss Pavelson

ISSN 1406-4723
ISBN 9985-59-556-4

CONTENTS

LIST OF PUBLICATIONS

This thesis is based on the following papers, which will be referred to in the text by their Roman numerals.

I Kononen, K., Kuparinen, J., Mäkela, K., Laanemets, J., *Pavelson, J.* and Nõmmann, S. (1996). Initiation of cyanobacterial blooms in a frontal region at the entrance to the Gulf of Finland, Baltic Sea. – Limnology and Oceanography, 41, 98–112.

II *Pavelson, J.*, Laanemets, J., Kononen, K. and Nõmmann, S. (1997). Quasi-permanent density front at the entrance to the Gulf of Finland: response to wind forcing. – Continental Shelf Research, 17, 253–265.

III Laanemets, J., Kononen, K. and *Pavelson, J.* (1997). Nutrient intrusions at the entrance area to the Gulf of Finland. – Boreal Environment Research, 2, 337–344.

IV Kononen, K., Hällfors, S., Kokkonen, M., Kuosa, H., Laanemets, J., *Pavelson, J.* and Autio, R. (1998). Development of a subsurface chlorophyll maximum at the entrance to the Gulf of Finland, Baltic Sea. – Limnology and Oceanography, 43, 1089–1106.

V *Pavelson, J.*, Kononen, K. and Laanemets, J. (1999). Chlorophyll distribution patchiness caused by hydrodynamical processes: a case study in the Baltic Sea. – ICES Journal of Marine Science, 56 Supplement, 87–99.

VI Kononen, K., Huttunen, M., Kanoshina, I., Laanemets, J., Moisander, P. and *Pavelson, J.* (1999). Spatial and temporal variability of dinoflagellate-cyanobacterium community under a complex hydrodynamical influence: a case study at the entrance to the Gulf of Finland. – Marine Ecology Progress Series, 186, 43–57.

VII Kononen, K., Huttunen, M., Hallfors, S., Gentien, P., Lunven, M., Huttula, T., Laanemets, J., Lilover, M.-J., *Pavelson, J.* and Stips, A. (2003). Development of a deep chlorophyll maximum of *Heterocapsa triquetra* Ehrenb. at the entrance to the Gulf of Finland. – Limnology and Oceanography, 48(2), 594–607.

VIII Laanemets, J., Kononen, K., *Pavelson, J.* and Poutanen, E.-L. (2004). Vertical location of seasonal nutriclines in the western Gulf of Finland. – Journal of Marine Systems, 52, 1–13.

IX Laanemets, J., *Pavelson, J.*, Lips, U. and Kononen, K. (2005). Downwelling related mesoscale motions at the entrance to the Gulf of Finland: observations and diagnosis. – Oceanological and Hydrobiological Studies, 34(2), 15–36.

X Vahtera, E., Laanemets, J., *Pavelson, J.*, Huttunen, M. and Kononen, K. Effect of upwelling on the pelagic environment and bloom-forming cyanobacteria in the western Gulf of Finland, Baltic Sea. – Journal of Marine Systems, submitted.

Some unpublished data are also presented.

INTRODUCTION

The Gulf of Finland (GOF), a shallow and elongated estuarine-like basin, lies in the north-eastern part of the tide less Baltic Sea. The gulf is about 400 km long, its width varies between 48 and 135 km and its total volume is ~1100 km^3 (~5% of the total volume of the Baltic Sea). The along-axis depth of the gulf decreases almost monotonically from 80–110 m at its entrance to 20–30 m in the eastern part. However, the bottom topography as a whole is complicated, particularly in the coastal areas of the gulf. There are two main contributors to the water exchange in the gulf: the freshwater discharge of larger rivers and the saltier northern Baltic Proper water intrusion. The annual freshwater runoff (mainly the River Neva) is ~110 km^3 and the water renewal time of the gulf is estimated to be less than 2 years (HELCOM, 1990). The large river inflow causes the surface layer salinity to decrease from 6–7 at the entrance to ~1 in the estuary of River Neva. The mean surface circulation in the GOF is weak and cyclonic (Alenius et al., 1998 and references therein), i.e. the eastward flow of the northern Baltic Proper water occurs along the Estonian coast and the opposite flow of the gulf water along the Finnish coast. At shorter time scales the current system is often more complicated, while the deviations from the mean scheme are mainly caused by the changes of the wind field.

The vertical thermal stratification in the GOF has a highly seasonal character. The water body is well mixed down to 50–70 m during winter. The solar heating and wind mixing form a sharp seasonal thermocline/pycnocline at a depth of about 10–15 m starting from May. The seasonal thermocline is the strongest in July–August, when the temperature difference between the warm upper mixed layer and the cold intermediate layer varies within 12–20 ºC. The haline stratification has weaker seasonality, but changes largely along the gulf. In the western GOF, as the continuation of the Baltic Proper, the permanent halocline with the salinity difference of 2–3 is centred at about 60 m depth. The eastern part of the gulf is characterised by a nearly linear increase of salinity from the surface layer towards the bottom.

As a result of phytoplankton primary production a seasonal course has also been recognised in the upper layer nutrient concentration: from the winter maximum values to the minimum in summer (HELCOM, 2002). In the Baltic Proper and GOF the primary production is limited by nitrogen (e.g. Granéli et al., 1990) and therefore the depleted stage of dissolved inorganic nitrogen (DIN) in the euphotic layer becomes after the spring bloom (dominantly diatoms and dinoflagellates), in the middle of May. The dissolved inorganic phosphorus (DIP) concentration usually reaches the minimum value before the late summer phytoplankton (mainly cyanobacteria) bloom, from the end of June to the middle of July. Below the nutrient-depleted euphotic layer the concentrations rapidly increase and analogically to the thermohaline stratification, the names of layers such as phosphacline and nitracline are widely used.

In the Baltic Sea the summer phytoplankton bloom usually occurs in July–August, when planktonic production is based mainly on regeneration and is controlled by nutrient availability and grazing (Kivi et al., 1993). The Baltic Sea

is also known as a basin with recurrent heavy late summer cyanobacteria blooms (Kononen, 1992). These blooms are possible because they are formed by nitrogen-fixing cyanobacteria, which are able to overcome nutrient limitation by fixing molecular nitrogen. The dominant species of cyanobacteria, *Nodularia spumigena* Mertens and *Aphanizomenon flos-aquae* (L.) Ralfs have been studied quite intensively. A considerable effort has been made to explain the increase of biomass and the extent of cyanobacteria blooms in the GOF during the last decade (e.g. Kahru et al., 2000; Pitkänen et al., 2001). Also, the hydrodynamical and meteorological factors controlling the cyanobacteria bloom development were under examination (e.g. Wasmund, 1997; Kanoshina et al., 2003).

The aim of the present thesis is to summarise the main results that are based on the field data of summers 1992–1999 and published in a series of articles. The data were collected and analysed together with scientists from the Finnish Institute of Marine Research (FIMR) under the leadership of Dr. Kaisa Kononen. In all years the experiments were interdisciplinary, i.e. included physical, chemical and biological measurements, with emphasis on the problems of the late summer cyanobacterial bloom. The data set is unique because it embraced the same area, the westernmost part of the GOF, and the same time of the season. Also, in several years we succeeded in timing to follow the development of mesoscale physical phenomena such as up- and downwelling, fronts and eddies. These ten-days to three-weeks case-orientated investigations are a considerable contribution to the knowledge of the GOF physics, which was reviewed earlier by Alenius et al. (1998). At the same time the mesoscale background served as a good basis for a better understanding of the spatial distribution of nutrients, as well as for the test of hypotheses of the initiation and development of phytoplankton blooms.

The content of the thesis is as follows. In Chapter 1 an introduction to the multiscale nature of the oceanic motions with reference to the mesoscale processes in the Baltic Sea is presented. Also, a general description of the study area in the western GOF and an overview of the observation strategy and data used are given. Chapter 2, the main part of the thesis, is devoted to the different mesoscale processes and to some aspects such as their generation, spatial structure, development, etc. This part is based on the results obtained from the different process-orientated field measurements. In Chapter 3 the main characteristics of the nutrient distribution (vertical location of nutriclines, intrusions) are analysed and the role of physical processes is determined. Chapter 4 deals with the initiation and development of cyanobacteria blooms and other specific phytoplankton biomass accumulations (subsurface and deep chlorophyll maxima).

1. PROCESS SCALES AND DATA ACQUISITION

1.1. Scales of physical processes

A large variety of motions/processes in a wide range of scales have been recognised in the world ocean. All the oceanic motions reflect the impact of atmospheric processes, while the input of energy from the atmosphere occurs in three main spatial scale ranges (e.g. Monin et al., 1977). The large-scale range ($\sim 10^6$ m) includes the global wind field controlled by the atmospheric cyclonic activity and differential heating between the poles and the equator. The meso-scale range ($\sim 10^4$ m) embraces sub-cyclonical wind variability, but also the tides. Through the small-scale range ($\sim 10^1$ m) the energy is channelled mainly to the wind waves. The most reasonable classification of oceanic variability bases on the dominating temporal and spatial scales. For example, Kamenkovich et al. (1986) divided the processes into the following horizontal scale order ranges: (1) $10^{-4}\ldots10^2$ m – *small-scale processes* (quasi-isotropic turbulence, surface waves etc.), (2) $10^2\ldots10^4$ m – *mesoscale processes* (internal waves, inertial oscillations, tides), (3) $10^4\ldots10^5$ m – *synoptic scale processes* (eddies, fronts etc.) and (4) $>10^6$ m – *global scale processes* (seasonal variations, quasi-permanent currents). In spite of the logical naming of these process groups, the term 'mesoscale' instead of 'synoptic scale' was widely used in the literature just to denote processes with the scales of the order of tens and hundreds of kilometres during the last decades. Therefore, hereafter this term is also used in the present study.

The mesoscale variability is characterised by the horizontal scales of the order of internal Rossby deformation radius $R_\mathrm{d} = NH/f$, where N is the mean buoyancy frequency, f is the inertial frequency (Coriolis parameter) and H is the depth. The internal Rossby radius indicates the horizontal scale at which Earth rotation effects become as important as buoyancy effects. As seen from the definition, R_d is sensitive to the vertical stratification and to the depth of the sea. In the oceans at mid-latitudes the typical R_d value is about 50 km ($H \approx 5$ km, $N \approx 10^{-3}$ s^{-1}). In the Baltic Sea, which is a shallow sea with different depths of sub-basins and with a strong seasonal course of stratification, the Rossby radius is considerably smaller and very variable. For example, an average (over about one decade) internal Rossby radius for the summer season of 5.2 ± 0.7 km was found in the Baltic Proper (Fennel et al., 1991), but a much higher value of 10.9 ± 0.4 km was determined in the Gotland Deep (Alenius et al., 2003). An extensive investigation in the GOF reveals the typical Rossby radii of 2–4 km, while in the deeper western part they are up to 5 km (Alenius et al., 2003).

The observations show that the scale of mesoscale processes usually equals a few times Rossby radius (e.g. Aitsam and Elken, 1982; Kamenkovich et al., 1986). Thus, in the western GOF the mesoscale range is approximately 5–20 km. The time scale of the mesoscale variability in the Baltic Sea has been estimated from a few days to a few weeks. It is definitely shorter than the time scale in the ocean given from weeks to months (Kamenkovich et al., 1986). To conclude, the mesoscale processes in the Baltic are small and short compared to

those in the ocean and therefore can be more 'conveniently' studied. However, both scales must be taken into account when planning the grid of the spatio-temporal field measurements.

1.2. Study area

All field measurements were carried out in the westernmost part of the GOF between longitudes 22°E and 24°E (Fig. 1). The study area extended about 50 km to the west from the more often used border of the GOF (line between Hanko and Osmussaar). Therefore, it represents well also the entrance area to the gulf. This region is characterised by a relatively narrow (15–30 km) along-gulf trench of 80–110 m depth (123 m as maximum) and with the positioning closer to the Estonian coast. The transition to the shallow coastal sea is also much steeper to the south from the trench. The sea areas at the Finnish coast and to the north from Hiiumaa Island are wider, but shallow (20–50 m) and with a complex bottom topography. The Finnish coastline is relatively smooth with the Hanko Peninsula as an exception. The Estonian mainland coast and the islands of Vormsi and Hiiumaa as its conventional extension form a more irregular configuration.

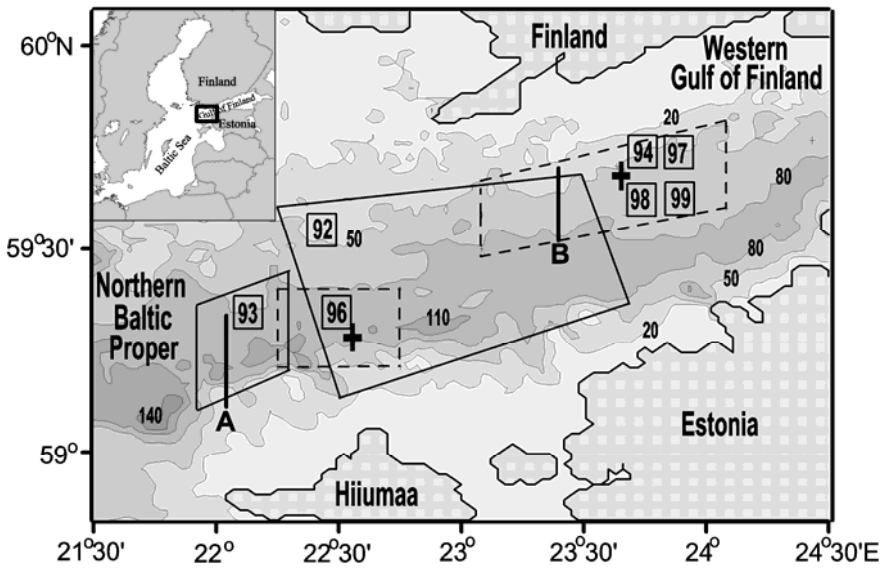

Figure 1. Map of the study area. The areas of mesoscale mappings for different years are bordered by solid or dashed lines and are supplied by the year numbers in small squares. Transects in 1993 and 1994 are represented by thick solid line (A and B, respectively). The crosses indicate the positions of anchor stations: at left – in 1996 and at right – in 1997–1999.

The wind field over the Baltic Sea is promoted by the mostly eastward moving atmospheric cyclones. A statistics of 40-years time series in the northern Baltic Proper and the western GOF revealed a dominance of S–W winds with a speed of >5 m s^{-1} (Soomere and Keevallik, 2003). The strong winds (>10 m s^{-1}) capable of forcing up- and downwelling were directionally even more concentrated around SW (Utö and Hanko). Another significant peak of the strong winds from E, also favourable for up- and downwelling cycles, was found in Hanko. It was concluded that data for Hanko represent well the wind regime of the western GOF.

Compared to the other Baltic Sea sub-basins there is no sill at the entrance to the GOF. Therefore, a permanent halocline exists in the whole deep of the study area. The almost stable vertical haline structure could be affected by the major inflows of salt waters into the Baltic Sea. For example, an increase of salinity in deep layers was observed about 18 months after the inflow in 1993 (Alenius et al., 1998). Also, a shorter time strong weakening of halocline is possible, which is caused by the estuarine flow reversal in the cases the SW wind component considerably exceeds the mean value (Elken et al., 2003).

A prominent phenomenon in the entrance area to the GOF is the quasi-permanent salinity front, which is a transition between the inflowing saltier water of the northern Baltic Proper and the outflowing fresher gulf water. Still, the front and the related circulation pattern have not been sufficiently studied and therefore only crude descriptions are available (see Section 2.1). A moderate quasi-steady eastward coastal current north of the central axis of the gulf has been observed and noticed in the modelling results (FIMR, unpublished data; Andrejev et al., 2004). The quasi-steady character of the current was explained by the baroclinic adjustment along a sloping bottom (Stipa, 2004).

1.3. Measurements

Data were collected during seven multidisciplinary studies (1992–1999) on board R/V *Aranda* (FIMR) in the western GOF (Fig. 1). The main task of these studies was to investigate the influence of the mesoscale physical processes on the initiation and development of cyanobacteria blooms and patchiness of the spatial distribution of phytoplankton. Therefore, the sampling stations and surrounding hydrographic survey areas were mostly chosen close to the coastal slope where wind forced physical phenomena are often well pronounced.

In 1992, the measurements of hydrographic (temperature and salinity) fields (NBIS Mark V CTD profiler) and the sampling of biological-chemical parameters were carried out on three cross-gulf transects with five stations on each. Since 1993, the research strategy was generally as follows: the mesoscale background mappings of hydrographic fields alternated by the periods of hydrographical–biological–chemical sampling along the fixed transect or at the anchor station (Fig. 1). The temperature and salinity were mapped with a towed undulating (0–50 m) system containing a NBIS Mark III CTD profiler and since 1994 an Electro-Optic Suarez fluorimeter. The mappings consisted of 5–10 parallel legs, 10–20 km long, ~5 km apart and ~600 m spacing between the

successive profiles. In addition, during the mesoscale mappings a ship's flow-through system recorded temperature and collected samples from a depth of 5 m for determination of nutrients, phytoplankton and chlorophyll *a* (Chl *a*).

At the anchor stations the hydrographical–biological–chemical sampling (duration from one to two days) was periodically carried out. The nutrient profiles were sampled at the standard depths and complemented by the additional samples from the nutricline layer during the majority of studies. The samples for the phytoplankton cell-counts, Chl *a* concentration measurements and primary production capacity determination were collected from different depth and time intervals, depending on the background conditions. The description of analytical methods for the determination of the chemical and biological parameters in the different cruises is presented in the corresponding articles (see Publications).

In some years background current velocity data were acquired by the ship-mounted ADCP (RDI NB, 150 kHz, bottom-track mode). Also, the moorings with current meters Aanderaa RCM-4, RCM-6 or RCM-7 at different depth and bottom-mounted ADCP (RDI NB 600 kHz) were deployed for some study periods. The meteorological data were recorded by the R/V *Aranda* weather station and in some years were complemented by Utö weather station data (Finnish Meteorological Institute). The general information about the measurements and mesoscale physical processes observed during the different studies is included in Table 1.

Table 1. The year and date of measurements, number of mesoscale mappings and physical phenomena observed in the study area and the relevant publications. In the column 'No. of mappings' the first number shows the total number of mesoscale mappings conducted by different systems and the second number indicates mappings performed only with a towed undulating CTD/fluorimeter.

Year	Date	No. of mappings	Mesoscale physical phenomena/situation	Publications
1992	2–13.08	4/–	upwelling, downwelling	VIII
1993	12–23.07	10/9	front	I, II, VIII
1994	21.07–3.08	11/10	low mesoscale activity	III, IV, VIII
1996	15–26.07	10/9	downwelling, eddy, front	V, VI, VIII, IX
1997	14-26.07	5/5	low mesoscale activity	VIII
1998	13–31.07	8/8	upwelling, eddy	VII, VIII
1999	19.07–11.08	10/3	upwelling	VIII, X

2. MESOSCALE PHYSICAL PROCESSES

2.1. Fronts

The Baltic Sea is rich in fronts, which separate the water masses with different properties. The diversity of water masses follows from the estuarine-like character of the Baltic, the circulation in and between the sub-basins and the vigorous modulation by the coastal processes. Therefore, fronts can be found over the whole water column, but those in the upper layer are best studied because of their biological–chemical consequences. Nevertheless, the internal fronts are of importance too when resolving horizontal mixing in the deeper layers. A thorough overview and classification of fronts in the word ocean was proposed by Fedorov (1986). Following his example, the main types of the Baltic Sea upper layer fronts were given on the basis of statistics of the repeated long thermohaline sections (Pavelson, 1988). The main types are: (1) *quasi-permanent salinity front* at the entrance to the larger gulfs or those related to the general circulation in a certain sub-basin, (2) *mesoscale salinity front* as the most frequent one found everywhere in the Baltic, (3) *temperature front* formed more likely by the interplay of water masses of different thermal stratification (a rare phenomenon), (4) *density-compensated front* with sometimes considerable cross-front temperature and salinity differences, and (5) wind-forced *upwelling front* in the coastal zones with high temperature differences and gradients. The most prominent one, a quasi-permanent salinity front at the entrance to the GOF, results well also from the model simulations (Elken, 1994; Andrejev et al., 2004).

An inspection of the GOF along-axis repeated transects revealed the dominance of randomly distributed mesoscale salinity fronts (upwelling fronts were not counted) and the quasi-permanent salinity fronts at the western boundary of sub-basins of the gulf (unpublished data from 1989–1990). The mean salinity differences of these front types were 0.31 ± 0.04 ($n = 77$) and 0.53 ± 0.12 ($n = 13$), respectively. The approximate width (due to multi-directional crossing) of the both front types was 2–5 km. The cross-frontal density gradient and the slope of the front to the sea surface are an indirect measure of the along-front current velocity, if the geostrophic adjustment is assumed. Considering the mean density difference of 0.50 kg m^{-3} and the typical slope to the sea surface of ~0.005 for the quasi-permanent fronts, the along-front geostrophic velocities were on the levels of 0.15–0.20 m s^{-1}. In spite of the favourable preconditions for the frequent occurrence of fronts in the GOF (confirmed by the above-mentioned data), only a few documentations can be found in the literature (e.g. Kononen and Nõmmann, 1992; Talpsepp, 1993). It is worth mentioning that the quasi-permanent salinity fronts related to the sub-basins of the GOF were also observed by Kononen and Nõmmann (1992).

A detailed investigation of the quasi-permanent salinity/density front in the entrance area to the GOF was performed during 12 days in July 1993 (II). The frontal zone was repeatedly mapped northwest of Hiiumaa. The front was predominantly orientated in a SW–NE direction and separated saltier waters

(6.5–6.8) of the northern Baltic Proper spreading along the Estonian coast and fresher waters (5.8–6.2) originating from the GOF. Due to the moderate heterogeneity of the water masses, the cross-front salinity and density differences varied in the range 0.4–1.0 (II, Fig. 3) and 0.3–0.6 kg m^{-3}, respectively. The mean cross-front gradients of salinity and density, considering the width of the front of 1.5–5 km, were 0.15–0.2 km^{-1} and 0.1–0.15 kg m^{-3} m^{-1}, respectively. The estimates of the slope of the front to the sea surface were within a relatively wide range of 0.003–0.01. Taking into account the typical values of the density gradient and the slope, the related velocities of the geostrophic current varied between 0.15 and 0.25 m s^{-1}. The existence of the jet current inshore the front was supported by the ADCP measurements (unpublished data).

The location of the front at the sea surface changed considerably during the study period (II, Fig. 5). After involving the wind data the following tendencies in the frontal zone were found: (1) under the conditions of easterly winds, the denser (saltier) water mass moved offshore, and the front became sharp and was strongly inclined to the sea surface (II, Fig. 4a), and (2) during westerly winds, the less dense water mass overrode onshore the denser water mass creating a secondary pycnocline approximately in the middle of the upper layer (II, Fig. 4b). Both patterns were repeated twice during the study period, following switches of wind direction, between E–NE and W–SW (both nearly parallel to the front). The response of the front to the changes of wind direction was relatively rapid and the characteristic cross-shore advection speeds were 0.15–0.2 m s^{-1}.

Wind-induced changes in the frontal structure were qualified using a semi-empirical physical model (e.g. Oey et al., 1987; Blanton et al., 1989), which bases on the concept that spatio-temporal changes of stratification reflect the response of the sea to different forcing. As a measure of stratification, the potential energy (PE) of water column relative to its well-mixed state was used:

$$\mathrm{PE} = g \int_{-h}^{0} (\rho - \langle\rho\rangle) z \, \mathrm{d}z, \tag{1}$$

where $\rho = \rho(z)$ is the density, g is the acceleration of gravity and $\langle\rangle$ denotes vertical averaging over water column of depth h. After simplifications (evaporation, precipitation, surface heat fluxes and tides are negligible), a non-dimensional equation describing how the changes of stratification, i.e. the rate of change of potential energy PE_t, is balanced by the wind-induced mixing and differential advection can be obtained:

$$(\mathrm{PE})_t / W_\mathrm{p} = \gamma + \rho_y (gh)^{1/2} / (2f\rho_0)[(gh)^{1/2} \tau^x / W_\mathrm{p}], \tag{2}$$

where $W_\mathrm{p} = \rho_\mathrm{a} C_\mathrm{a} |\boldsymbol{u}_\mathrm{a}|^3$ is the wind power, γ is the constant dimensionless wind mixing efficiency parameter, ρ_y is constant cross-front density gradient, ρ_0 is a reference density for seawater, τ^x is the along-front wind stress, C_a is the wind drag coefficient, ρ_a is the density of air and $\boldsymbol{u}_\mathrm{a}$ is the wind velocity vector. A relatively good correlation was found between W_p and PE calculated from the measured density and wind data over the whole study period (II, cf. Fig. 7a and

b). Also, the calculated non-dimensional PE vs. the wind-induced advection parameter in general followed the model relationship (II, Fig. 8). The discrepancy from the model in some cases was explained by an along-front advection, i.e. considering the inner variability of the main water masses.

A complicated horizontal structure of the salinity fronts in the upper layer was followed during a 10-days study north of Hiiumaa Island in 1996 (V). A well-pronounced moderate front with the salinity difference of ~0.3 can be also interpreted as a part of the GOF entrance quasi-permanent front. The front evolved through continuous meandering and therefore moved back and forth in its cross-axis direction (V, Fig. 2a–e). The current velocities in the frontal zone reached up to 0.30 m s^{-1} (12 m depth) and were directed towards the inner gulf. Similarly to the development of currents in the deeper layer (see Section 2.3), the frontal current transformed to an anticyclonic circulation, i.e. an eddy (V, Fig. 2d–h). Simultaneously, fresh water probably originating from the shallow sea east from Hiiumaa Island was entrained by the eddy in its periphery. Thus, the saltier water became 'arrested' and a salinity front formed at the edge of the eddy. In the area outside the eddy, where the main front was initially located, a gradual smoothing of the horizontal salinity distribution occurred (V, Fig. 2e,f,h). Therefore, the instability of frontal currents (resulting e.g. in the formation of an eddy) can be hypothesised as a possible mechanism of destroying the quasi-permanent front in its eastern parts.

2.2. Upwelling

The coastal upwelling, forced by alongshore winds (with coast on the left in the northern hemisphere), is expressed as an offshore Ekman transport in the upper layer and a compensating lift of cold water from the lower layers to the surface. Wind-induced coastal upwelling is either a quasi-persistent phenomenon driven by large-scale meteorological patterns, or a temporary event forced by variable wind with time scales from a few days to a week. In the former case, upwelling lasts for months with more or less continuous input of nutrients into the upper mixed layer causing efficient primary production in many regions of the world ocean (Mann and Lazier, 1991). Time-variable wind forced upwellings are characterised by the periods of onset of upwelling, alternated by warming of cold upwelled water when the wind relaxes or reverses. The filaments of upwelled water extending far from the upwelling front are often recognised and classified by their nature, but the discussion of their generation mechanisms is still open (Strub et al., 1991). The surface boundary layer dynamics in coastal regions is strongly influenced by the bottom and coastal topography, and therefore the locations of upwelling centres and filaments may be highly repeatable (Huthnance, 1995).

Considering the directional distribution of stronger winds in the GOF (Soomere and Keevallik, 2003), the upwelling is mainly expected at the Finnish coast. A few documentations of measured upwelling in the GOF can be found in the literature (e.g. Haapala, 1994; Talpsepp et al., 1994). These studies describe upwelling events at the Finnish coast with an essential decrease of water

temperature and an increase of nutrient concentrations. A relationship between buoyancy (stratification) and wind impulse from the series of different upwelling events as well as the minimum wind speed and duration criteria for the generation of upwelling events under different buoyancy conditions were obtained (Haapala, 1994). Statistical analysis of a series of satellite sea surface temperature (SST) images of the GOF area also revealed a clear dominance of upwelling along the Finnish coastal zone and the pronounced upwelling filaments sometimes extending to the Estonian waters (Kahru et al., 1995). The observation data are supported by model simulations (Myrberg and Andrejev, 2003; Andrejev et al., 2004), which expose the frequent upwelling area, with about 200 km in length and 5–15 km in width, in the western GOF.

An intensive measurement campaign to study the upwelling at the Finnish coast was carried out in July–August 1999 (X). Two upwelling events with an interval of about three weeks were promoted by the strong alongshore westerly wind pulses with a duration of 2 and 7 days and with a speed of 7–12 and 7–14 m s^{-1}, respectively. During the rest periods the winds were relatively low. In both cases the upwelled water covered practically the whole northern part of the GOF and the filaments extended to the central gulf (X, Fig. 3). A similar upwelling pattern was also followed in the satellite SST imagery of July 1998. The most striking feature on all images (1998 and 1999) is the along-gulf location of filaments nearly in the same locations. This supports the idea of the formation of the filaments through the upwelling front instabilities caused by the varying bottom topography and/or indented coastline.

The second upwelling with a filament was mapped 9 times during three weeks, i.e. the formation, development and post-relaxation phases were followed (X, Fig. 4). The first signs of upwelling as a few degrees colder water than the surrounding water (18–19 ºC) appeared about one day after the strengthening of the wind. Due to continuing strong westerly winds, the offshore widening of the upwelling zone and the most pronounced stage of this upwelling event four days later with near-coast surface layer temperature of 8 ºC were observed in the study window. The rapid decrease of the wind followed by a relatively low wind period caused a relaxation of the upwelling and the warming of surface waters. In the relaxation phase the 'normal' seasonal stratification re-established, but the filament of colder water was still observed during the last mapping (about two weeks after the relaxation of the wind). A similar tendency was followed after the first upwelling event, thus, both upwelling filaments had approximately the same time scale of three weeks. This is in accordance with the estimate obtained from the formula of diffusive lifetime $t_d = 0.5L^2K^{-1}$ of thermohaline intrusion (Stommel and Fedorov, 1967). Here L is the horizontal cross-filament scale and K is the horizontal eddy diffusivity. Taking L = 10 km and K = 30 m^2 s^{-1} (Andrejev et al., 2004), the lifetime of the filament would be about 19 days. Although the estimate is approximate, it also shows that the horizontal mixing is a slow process with the time-scale likely in several weeks.

The intensive upwelling stage was characterised by a sharp front with a density difference of 0.4–0.9 kg m^{-3} and a width of 2–3 km. As the mean cross-front density gradient was 0.25 kg m^{-3} m^{-1}, the mean eastward geostrophic current associated to the front is ~0.25 m s^{-1}. This current presumably counteracts the westward quasi-steady current along the bottom slope (Stipa, 2004), as was observed during a weaker upwelling event in the same area in 1998 (VII, Fig. 3). Before the upwelling event the currents in the upper (8 m) and lower (25 m) layers with velocities of ~0.10 m s^{-1} were both directed along-shore (WSW). After the setup of the wind favourable to upwelling, the current in the lower layer remarkably weakened, but still flew westward. In the upper layer, due to Ekman transport, the current turned offshore (SE), with typical velocities of 0.05–0.10 m s^{-1}.

The upwelling event changed drastically the horizontal distributions of nutrient and Chl *a* concentration in 1999 (X, Fig. 4). The consecutive mappings showed the propagation of phosphate-rich upwelled water to the study area in accordance with the development of the temperature distribution. In the coldest water, north from the upwelling front, the maximum phosphate concentration in the subsurface layer was as high as 0.32 mmol m^{-3}. After the relaxation of upwelling the phosphate concentrations decreased, but still clear contours of filament (~0.10 mmol m^{-3}) were observed for a week. The distributions of nitrate and silicate also followed the distribution of temperature, while the relatively weaker concentration of nitrate in the upwelled water is explained by the deeper location of nitracline compared to the phosphacline (see Section 3.1). During the active phase of the upwelling, the Chl *a* distribution was shaped by the upwelling front and concentrations of <2 mg m^{-3} were observed in the coastal upwelled water compared with 5–8 mg m^{-3} in the central GOF.

2.3. Downwelling

The downwelling events in the coastal sea develop as a response to the along-shore wind impulses (with coast on the right in the northern hemisphere). Conversely to the upwelling, downwelling is characterised by converging flows, i.e. an onshore Ekman transport and the sink of surface layer waters. Both upwelling and downwelling lead through geostrophic adjustment to the development of along-shore coastal jets. In general, the downwelling events have not been much studied although a large portion of substance (e.g. phytoplankton) could be drawn out from the surface layer. The model simulations have been devoted mainly to the development of the downwelling density front (e.g. Allen and Newberger, 1996) as well as to the upper layer dynamics during alternating upwelling–downwelling cycles (Carbonel, 2003). The downwelling associated jets have been found in geostrophic balance with the cross-shore pressure gradient and the horizontal scale of the jet is proportional to the square root of the horizontal diffusion coefficient (Feliks, 1991). The jets are sensitive to the coastline geometry and bottom topography, and as a result of the flow instability the formation of eddies is possible (Feliks and Ghil, 1993).

A few downwelling events have been mapped in the Estonian coastal zone of the GOF (Talpsepp, 1993; Talpsepp et al., 1994). These studies revealed the decline of the thermocline by 10–20 m and the presence of downwelling related jets. Direct current measurements showed a relatively strong along-shore eastward flow of 0.35 m s^{-1} above the declined thermocline during the downwelling period. Two days after the relaxation of the wind favouring downwelling the current reversed and decreased considerably. The occurrence of downwelling preferably at the southern coast of the GOF is caused by the dominating westerly winds. Also the model runs expose the dominance of downwelling (by means of the persistency index of the vertical velocity) at the Estonian coast (Myrberg and Andrejev, 2003).

Our field measurements in July 1996 enabled to study a whole intensive downwelling cycle to the north of Hiiumaa Island (IX). The strong westerly winds favourable to downwelling blew two days with the along-shore velocity component up to 13 m s^{-1} (corresponding wind stress component of 0.15–0.30 N m^{-2}) and the rest period was characterised by the relatively weak winds (IX, Fig. 2). The stable downwelling regime over the steep bottom slope was created during one day and it stayed about three days after the wind supporting downwelling subsided. In the downwelling zone the isolines in the thermocline declined from ~30 m depth in the open gulf down to 50–60 m on the bottom slope (IX, Fig. 3).

A downwelling-associated jet above the declined thermocline was centred at about 35–40 m depth and carried the saltier northern Baltic Proper water (salinity >6.9) north-eastward (IX, Fig. 4a–c). The mappings of current velocity by the ship's ADCP revealed a meandering character of the jet and the velocities in its core up to 0.30 m s^{-1} (IX, Fig. 5a,b). The width of the jet was 8–12 km, thus the offshore scale of the jet was 2–3 times of the internal Rossby deformation radius (~4 km). A rapid change in the development of the jet occurred during the relaxation phase of the downwelling. The dominantly cyclonically turned jet split, so that a pronounced anticyclonic on-shore branch was observed (IX, Fig. 5b). Simultaneously, to the west from the splitting area the current velocities gradually weakened (IX, Fig. 5b,c), which is also in accordance with the relaxation of the downwelling. Further the anticyclonic branch of the jet transformed into an eddy (see Section 2.4).

For better understanding of the three-dimensional circulation in the downwelling zone a coupled analysis of the measured density and current fields was performed (IX). It is known that the mesoscale processes influence substantially the upper sea structure inducing alternating cyclonic and anticyclonic vorticity bands (e.g. Pollard and Regier, 1990). The conservation of the potential vorticity of a water parcel leads to vertical motions, which modify the stratification of the seasonal thermocline. The relative geostrophic vorticity field, $\zeta_g = \partial v_g/\partial x - \partial u_g/\partial y = \nabla^2\psi$, was calculated from non-divergent streamfunction ψ (u_g and v_g are the geostrophic velocity components). The inshore part of the downwelling related jet appeared anticyclonicly sheared with the highest anticyclonic vorticity value of $-0.95f$ (IX, Fig. 8a). A moderate

cyclonic vorticity band with values up to 0.7*f* was located at the open gulf side of the jet. The anticyclonic branch of the jet after its splitting was reflected in the corresponding concentration of enhanced anticyclonic vorticity (IX, Fig. 8b). In some locations the relative vorticity contours were not parallel to the streamlines, which can be explained by the curvature of the flow field and by the corresponding contribution to the shear vorticity. Therefore, considerable vertical motions could be expected to conserve potential vorticity $(f + \zeta_g)/h$, where h is the water parcel depth, in regions of large gradients of relative vorticity along streamlines (Onken, 1992).

To estimate the vertical velocity the quasi-geostrophic ω-equation diagnostic technique with a solely vertical velocity forcing term, divergence of **Q**-vector (Hoskins et al., 1978), was used (IX, Eq. 4). The assumption of quasi-geostrophic balance is correct for mesoscale flows with Rossby numbers (ζ_g/f) of the order of 0.1. Nevertheless, a test of the ω-equation showed that it can be used even if the Rossby number is 1.2 (Pinot et al., 1996). Therefore, despite the weakness of the quasi-geostrophy assumption this method was widely used for the diagnosis of mesoscale vertical motions (e.g. Leach, 1987; Shearman et al., 1999). In our case (also relatively high Rossby numbers) the distribution of the **Q**-vector divergence revealed the cells of strong convergence and divergence along the downwelling related jet (IX, Fig. 10). Convergence (divergence) of **Q**-vector implies upwelling (downwelling) with a positive (negative) vertical velocity. The extreme values of the **Q**-vector convergence and divergence were up to -3.5×10^{-14} and 2.6×10^{-14} m^{-1} s^{-3}, respectively. The magnitude of vertical velocities was obtained from the ω-equation approximating the horizontal and vertical differentials by inverse length scales. Taking the vertical length scale of 10 m and horizontal length scale of 5 km, the corresponding maximum upward velocity was 4.1×10^{-4} m s^{-1} (35 m d^{-1}) and downward velocity was 3.1×10^{-4} m s^{-1} (26 m d^{-1}). The calculated velocities reflect the vertical disturbances of density surfaces as well as the vertical flow component along sloping density surfaces.

2.4. Eddies

Mesoscale eddies are coherent cyclonicly or anticyclonicly rotating structures in the ocean, transporting and mixing water with particular physical and biological properties. They can be formed by various mechanisms at different depths in the sea interior. The basic eddy forming mechanisms are related to the strong meandering currents (e.g. rings that pinch off from the Gulf Stream), baroclinic instability of the mean flow, influence of bottom topography on the currents and the direct impact of the wind field over the sea (Kamenkovich et al., 1986). A specific type of mesoscale eddies is Meddies, which are long-lived isolated salt lenses of Mediterranean origin propagating in the northeast Atlantic (e.g. Armi et al., 1989).

In the Baltic Sea the systematic field investigation of mesoscale eddies started in the late 1970s by means of repeated hydrographic mappings and current meter moorings (Aitsam and Elken, 1982; Aitsam and Talpsepp, 1982;

Aitsam et al., 1984). Both intra-halocline cyclonic and anticyclonic eddies with diameters of about 20 km were frequently found in the region of the Gotland Basin. More detailed data on eddies in the same basin were obtained during the PEX and DIAMIX experiments (Elken et al., 1994; Stigebrandt et al., 2002). In the Stolpe Channel and Gdansk Bay several smaller cyclonic eddies were observed in the intermediate layer (Zhurbas et al., 2004). Also several numerical modelling attempts have been made to simulate the formation of mesoscale eddies in the Baltic Sea (e.g. Lehmann, 1995; Elken, 1996; Zhurbas et al., 2004).

In the GOF observational as well as numerical studies of mesoscale eddies are practically absent. Only very few evidences of eddies can be found in the review of literature by Alenius et al. (1998). Therefore, the investigation of the formation and anatomy of an anticyclonic eddy in July 1996 (IX) is unique. The eddy formed after the rapid branching of the eastward downwelling related jet to the offshore cyclonic and the inshore anticyclonic branch (IX, Fig. 5b). The latter can be interpreted as an eddy in its formation stage, and afterwards a similar anticyclonic velocity pattern was observed until the end of the experiment (IX, Fig. 5d–f). The eddy was centred in the seasonal thermocline at about 30–35 m depth (IX, Fig. 6) and embraced the upper 70-m layer. The vertical density structure was typical of the geostrophically balanced anticyclonic eddy: doming isopycnals above and bowled ones below its central depth. The eddy core salinity, comparable to that in the jet core (IX, Fig. 4), only slightly decreased by the end of observations, which can be addressed to the mixing processes.

At the formation stage the typical velocities in the eddy were 0.15–0.2 m s^{-1} (IX, Fig. 5). A noticeable intensification of velocities in the periphery of the eddy occurred in about two days, which was interpreted as a jet-like ring flow 4–6 km wide and with maximum velocities in the core up to 0.35 m s^{-1}. The maximum velocity was observed at the depths of reversal in baroclinicity and the isopycnal displacements yielded slopes of the order of 10^{-3} (IX, Fig. 6a). A similar structure of density and velocity fields of anticyclonic eddies in the open Baltic had been observed by Aitsam et al. (1984) and in the ocean by e.g. Pingree and Le Cann (1992). The creation of reversed baroclinicity and an associated jet in the eddy detached from a meandering front and lying between the seasonal and main thermocline was modelled by Onken (1990).

From the mesoscale mappings the diameter of the eddy was estimated to be 15–20 km, which is four to five times the internal Rossby deformation radius. Another estimate, eddy radius of ~8 km, obtained from the geometrical considerations applied to the mooring station current data fully supports that. It was not possible to determine exactly the lifetime of the eddy because the mapping series was not enough long. Therefore, relying on some signs of the decay of the eddy by the last mapping, the lifetime from about ten days to a fortnight can be speculated.

The same salinity in the core of the downwelling jet (saltier northern Baltic Proper water) and successively in the eddy, both centred at about the same

depth, suggests that the eddy had formed from the anticyclonic branch of the jet. The formation mechanism is still unclear, but more likely it could be associated with the jet instability generated by the particular topographic features. The development of the jet to the eddy could be followed also on the maps of isopycnal potential vorticity (IPV). The IPV was calculated by combining the measured current and density fields as

$$\mathrm{IPV} = \frac{(f + \zeta_g)}{\Delta h} \frac{\Delta\rho}{\rho}, \tag{3}$$

where Δh represents the layer thickness between two selected isopycnals $\rho \pm \Delta\rho/2$ (e.g. vertical eddy boundaries). The conservation of the potential vorticity means that an increase (decrease) of the rotation rate ($f + \zeta_g$) in the layer between selected isopycnals is compensated by an increase (decrease) of the layer thickness. A tongue of low IPV values on the inshore side of the downwelling jet gradually advected eastward and transformed to the local IPV minimum representing the anticyclonic eddy (IX, Fig. 9e–h). These are the regions of weak stratification (Δh is large) and also of strong anticyclonic relative vorticity. The high IPV gradient, i.e. about 20-fold change over a distance of ~5 km (IX, Fig. 9g,h), appeared in the eddy periphery due to the remarkable increase of absolute vorticity and the decrease of layer thickness. The IPV front might act as a barrier restricting lateral mixing (Allen and Smeed, 1996), which could explain the retaining of the high salinity in the eddy core for at least a week.

The mesoscale eddies were also observed in the Finnish coastal zone in July 1998 (unpublished data). Two anticyclonic eddies at different locations with diameters of about 10 and 15 km were both centred in the seasonal thermocline. The larger eddy was characterised by strong velocities (up to 0.25 m s^{-1}) and its lifetime was evidently more than one week. The smaller eddy was relatively weak with the lifetime not exceeding 5 days. The possible formation of such eddies can be explained similarly to the conceptual model given by Peliz et al. (2002). The strong westerly winds periodically dominated in July and set up upwelling at the Finnish coast and an associated eastward jet current in the upper layer. To the south there is a westward current associated with the large-scale circulation in the gulf (Andrejev et al., 2004; Stipa, 2004). Therefore, an eddy found between these two currents would preferably have an anticyclonic character. The generation of eddies can be addressed to the interaction of these currents with the topographical features in the northern GOF. However, the problem of eddy generation needs further detailed field studies as well as numerical model simulations.

3. NUTRIENT FIELDS

3.1. Vertical location of nutriclines

The vertical distribution of nutrients in the GOF has been often determined (as a background for almost all biological studies) and therefore the general structure is known to the marine scientists. However, the summarising quantifications as well as explanations of the formation of nutriclines are absent. Revision of the nutrient data (350 profiles) collected during summer cruises in 1992-1999 allowed us to estimate the depth of main seasonal nutriclines (phosphacline, nitracline and silicocline) and elucidate their vertical separation (VIII). For the analysis the nutricline depth was defined as the shallowest depth where the nutrient concentration exceeds the mixed layer value by a prescribed concentration difference (0.05 mmol m^{-3} for phosphate and nitrate, and 0.5 mmol m^{-3} for silicate).

For most years the following depth ordering of the clines below the pycnocline was observed: silicocline, phosphacline and nitracline (VIII, Table 2). The year to year changes of pycnocline, silicocline and phosphacline depths were mainly similar. A considerable year to year variation, however, was observed for the depth of the nitracline. A deep nitracline, located at about 30 m depth, was observed in 1993, 1996 and 1998. In these years also the largest spacing between the phosphacline and nitracline occurred, being as large as 14 m in 1993 and 1998 (10 m in 1996). In the rest of the years the spacing between these clines was 4–5 m, which can be explained by the following arguments.

In the nitrogen limited Baltic Proper and GOF the winter DIN resources in the upper layer are consumed during the spring bloom while a considerable amount of DIP remains. It was shown that vertical mixing contributes about 50% of the net nutrient uptake in the euphotic zone during the spring bloom and the level of zero net consumption for nutrients is 15–25 m, which is considerably deeper than 1% light level (Lundberg and Rydberg, 1994). Simultaneously, high Chl *a* and very low nitrate+nitrite concentrations were measured at 20 m depth, also deeper than 1% light level (Fonselius and Valderrama, 1994). The seasonal thermocline starts to develop at the time of the spring bloom and acts as a barrier to the further mixing of nutrients into the upper layer. Thus we suppose that the usual depth of the nitracline of 14–25 m observed in summer (VIII, Table 2) was determined mainly by the vertical extent of the spring bloom in the water column. The period after the spring bloom until the late summer bloom is characterised by the development of a strong thermocline and the lowest phytoplankton biomass (e.g. HELCOM, 2002), which suggests that the vertical distribution of nitrate remains unchanged. The continuous decrease of the phosphate concentration to the detection level in the layer above the thermocline after the spring bloom can be explained by the maintenance of primary production (e.g. Rahm et al., 2000) and by storage of phosphate by the seed population of *Aphanizomenon* sp. (Larsson et al., 2001). The strong seasonal thermocline effectively restricts mixing and therefore it is more likely that a phosphacline forms in the upper

part of the thermocline. The seasonal thermocline in the western GOF lies typically above 15 m depth. Therefore, the usually observed separation of about 5 m between the phosphacline and the nitracline seems to be caused by the difference in the vertical extent of the spring bloom and the depth of the seasonal thermocline. The prerequisite for the separation is the low winter time DIN:DIP ratio in the upper layer.

The unusually deep nitracline (1993, 1996 and 1998) was located fairly well below the depth corresponding to 0.1% surface light intensity. In summers 1996 and 1998 cold and windy weather prevailed and surface layer temperature remained below 16ºC, less than optimum for bloom-forming cyanobacteria (Lehtimäki et al., 1997). In both years a heavy bloom of *Heterocapsa triquetra* dominated over the moderate bloom of more temperature tolerant cyanobacteria *Aphanizomenon* sp. It was shown that the bloom of vertically migrating *H. triquetra* in 1998 had been formed on the basis of the surplus phosphate in the surface layer and the nitrate pool in the thermocline (VII). The development of the bloom, therefore, led to the formation of a deep nitracline at about 25 m depth. Further, a pulse of phosphate into the surface layer, induced by wind mixing and an upwelling event, modified the physiological status and swimming behaviour of *H. triquetra* cells, and their migration continued downward. Cells of *H. triquetra* accumulated at the top of the nitracline and formed a deep chlorophyll maximum (see Section 4.3). As a result of the nitrate uptake of cells in dark, the nitracline was eroded deeper to a depth of 30–35 m. A similar scenario holds also for the formation of the deep nitracline after the relaxation of downwelling in 1996. This was proved by estimates of the *H. triquetra* biomass increase and available nitrogen and supported by the observed deep chlorophyll maximum dominated by *H. triquetra* at the top of the nitracline (V).

3.2. Effect of physical processes

The wind-driven mesoscale circulation led to significant vertical excursions of nutricline depths in the coastal sea area. The largest upward/downward displacements of clines occurred during upwelling/downwelling events. For example, the persistent westerly winds in 1992 caused the decline and lift of clines, which resulted in a large cross-gulf difference of phosphacline and nitracline depths, up to 25 m (VIII, Fig. 4). During the downwelling in 1996 the phosphacline and nitracline were found at a depth of about 40 m, where the clines were squeezed to each other (VIII, Fig. 5b). After the relaxation of the downwelling the both clines were lifted by ~15 m. The shallowest nutricline depths were estimated during a strong upwelling in 1999 (VIII, Table 2).

In the zone of the quasi-permanent salinity front considerable spatial and temporal variations of the depth of nutriclines were observed (VIII, Fig. 6). In the offshore side of the front the variations of depths of the phosphacline and nitracline were within 5 m and the spacing between the clines stayed at around 20 m for the whole study period. A strong deepening of the nitracline and a rise of the pycnocline and phosphacline were observed in the inshore side of the

front. The spacing between the phosphacline and the nitracline tripled within two days, and afterwards, by the end of the study, the initial depths of clines were re-established. These large changes in the vertical separation of the phosphacline and the nitracline can be explained by the wind forcing. The offshore/onshore movements of this front are controlled by easterly/westerly winds (II). Therefore the westerly wind caused an onshore Ekman transport in the upper layer as well as movement of the front and less saline open gulf water toward the coast. The transport was accompanied by a downwelling near the coast and the compensating offshore flow between the phosphacline and the nitracline below the inclined frontal interface. Such a cross-coast current system favoured a strong deepening of the nitracline and a rise of the phosphacline. The following easterly wind event caused an offshore Ekman transport in the upper layer with corresponding relaxation of the downwelling and initial arrangement of clines.

The enrichment of the upper mixed layer with nutrients by upwelling and turbulent mixing is highly dependent on the vertical separation of the phosphacline and the nitracline. In 1998, when the separation between the phosphacline and the nitracline was large, an upwelling event transported only phosphate into the upper mixed layer (VIII, Fig. 7). In 1999, the nitracline was twice shallower, thus much closer to the bottom of the upper mixed layer, and both phosphate and nitrate were brought into the surface layer.

The amount of nutrients transported into the upper layer via the turbulent mixing was calculated by the simplified diffusion equation

$$C_t = (K(z)\, C_z)_z\,, \tag{4}$$

where C is the nutrient concentration, $K(z)$ is the vertical eddy diffusivity, z is the vertical coordinate, t is the time and subscripts denote partial derivatives. A profile of $K(z)$ was obtained from the turbulence measurements in 1998 (Lilover et al., 2003). Comparison of the initial (measured) and over 1 day wind-forcing (wind speed of 11 m s^{-1}) calculated profiles shows that the increase of phosphate in the upper 10 m water column was 0.32 mmol m^{-2} while the amount of nitrate mixed into the upper layer is negligible (VIII, Fig. 8). If the nitracline was located closer to the surface so that the spacing between the phosphacline and the nitracline was 5 m, the increase of nitrate in the upper water column would be as large as 0.12 mmol m^{-2}.

3.3. Intrusions

Nutrient profiles sampled in the Finnish coastal sea area were characterised by a frequent occurrence of intrusions in the nutricline layer. Usually the cold and phosphate- and nitrate-rich intrusions were located above the warmer nutrient-poor water of the open GOF (III, Fig. 7; VIII, Fig. 3a). The mean thickness of both nutrient intrusions varied mainly within 4–9 m (VIII, Table 4). The mean intensity of phosphate intrusions did not change much (0.10–0.13 mmol m^{-3}) throughout all summers analysed, while the mean intensity of nitrate intrusions changed much more (0.32–1.28 mmol m^{-3}) from year to year. The high-resolution sampling (0.2 m interval) demonstrates also the presence of small-

scale nutrient intrusions with the thickness of tens of centimetres and lower intensity (VIII, Fig. 3b). Nutrient intrusions were found only in the Finnish coastal sea mainly in the depth interval of 20–30 m, while near the Estonian coast no intrusions were observed. This finding enables to relate the intrusions with the westward quasi-steady current along the sloping bottom to the north of the central axis of the gulf (see Section 1.2). In the GOF the isohalines and isopycnals are inclined to greater depths toward east (e.g. Alenius et al., 1998) as typical of the estuarine hydrography. Therefore, it can be assumed that the quasi-steady current carries colder and nutrient-rich water from the deeper layers along the inclined isopycnal surfaces. As a result an internal thermohaline/nutrient front forms, and instability of the front may lead to the generation of intrusions. A presence of such front in 1994 and enhanced intrusive layering to the south from that (III) support this hypothesis. The observed frequent occurrence of intrusions with the thickness from tens of centimetres to around ten metres hints to their essential role in inshore–offshore nutrient exchange.

4. SUMMER PHYTOPLANKTON BLOOMS

4.1. Initiation of cyanobacteria blooms

Cyanobacteria blooms occur from the end of June to the end of August, when the surface layer temperatures are high and the nutrients are most depleted. Cyanobacteria blooms have been related to low DIN:DIP ratios (e.g. Niemi, 1979; Laamanen and Kuosa, 2005) as well as to water temperature as the controlling factor (Lehtimäki et al., 1997; Wasmund, 1997). In general, in the GOF the phytoplankton growth and biomass are nitrogen limited (e.g. Graneli et al., 1990; Lignell et al., 2003), an exception being the filamentous cyanobacteria that can fix atmospheric nitrogen. Therefore, because of competative ability provided by nitrogen fixation, nutrient pulses of phosphorus of different origin (e.g. upwelling) with low DIN:DIP ratios would be expected to favour cyanobacteria. Other sources, such as intracellular storage of spring bloom excess phosphate and remineralisation of the upper layer phosphorus pool, were also found important in the formation of cyanobacteria blooms (Larsson et al., 2001; Lignell et al., 2003). Below physical mechanisms leading to the initiation of the cyanobacteria blooms are described.

4.1.1. Processes in the frontal zone

The frontal zone of a quasi-permanent front at the entrance to the GOF was characterised by the differential advection of water masses (see Section 2.1). The westerly winds supported the flow of less saline/dense water toward the shore over the saltier water mass. As a result, a secondary pycnocline was formed, creating a relatively shallow (2–5 m) subsurface mixed layer for two days (I, Fig. 3B). Phytoplankton communities associated with the main water masses before the formation of the isolated subsurface layer were clearly different, while the abundance of *Aphanizomenon* and *Nodularia* was relatively low in the both water masses. Primary productivity and assimilation number

(primary productivity/Chl *a*) in the >20 μm size fraction (represents cyanobacteria) notably increased when the overriding less saline water formed a shallow mixed layer (I, Fig. 10, 11). Further, the productivity in the same size fraction stayed high most likely due to solar heating and low wind speed, which are favourable conditions in forming a diurnal secondary pycnocline. When confined to a shallow mixed layer, plankton organisms are exposed to higher quantities of irradiance, which may cause an inhibitory effect on the production. Nevertheless, a rapid and continuous increase in the abundance of *Nodularia* after the formation of a shallow layer (I, Fig. 12B) seemed to have a stimulating rather than inhibitory effect on the production of this species. There was also an overall continuous warming of the upper layer from ~15 to 17 ºC during the observation period. These temperatures are well below the optimum temperature for the growth of *Nodularia*, 25–28 ºC (Lehtimäki et al., 1997), but the higher ones exceed the germination temperature of the species, 16 ºC (Kononen, 1992). However, it remains unclear whether the observed initiation and vigorous growth stimulation of *Nodularia* bloom was ultimately caused by increased irradiance and/or increased temperature. The secondary pycnocline prevented vertical nutrient pulses into the surface layer. It is therefore likely that the *Nodularia* bloom was able to benefit from the low DIN:DIP ratio prevailing before the onset of the bloom.

The temporal course of the abundance of *Aphanizomenon* was characterised by two increasing periods (I, Fig. 12A), with the abundance being noticeably higher in the inshore high saline water mass than in the less saline water mass. This finding means that the quasi-permanent front, with a moderate (geostrophic) jet current of ~0.20 m s^{-1} on its saltier side, formed a boundary between two environments that were differently supplied by the nutrients. The increases of the abundance of *Aphanizomenon* were almost coherent with the pattern of stronger wind events, and this aroused an idea of possible wind-induced mixing of phosphate into the upper mixed layer on the saltier side of the front.

It is known that the seasonal pycnocline effectively restricts vertical transport of nutrients into the upper mixed layer. The amount of energy required to mix nutrients into the upper mixed layer depends on the intensity of the seasonal pycnocline and the depth of nutriclines. The potential energy of the water column above this depth relative to its well-mixed state |PE| (Eq. 1) can be used as a measure of the amount of energy required to mix this water column, i.e. the energy barrier. The density difference from the sea surface to the minimum depth at which the concentration of DIP clearly increased (DIP > 0.1 μm) was reduced to 0.5 ± 0.3 kg m^{-3} at the station nearest to the coast (saltier water), compared with 1.7 ± 0.2 kg m^{-3} on the less saline side of the front (I, Fig. 5B). For the nearshore station, the values of |PE| were mainly in the range 20–60 J m^{-2}, although larger values (up to 230 J m^{-2}) appeared when the front was almost horizontal, thus increasing the stratification. On the less saline side of the front, the values of |PE| were much higher, varying from ~300 to 1200 J m^{-2}. The amount of wind energy that is converted into the change of

potential energy of a water column through the turbulent fluxes was estimated from the wind power $W_p = \rho_a C u^3$ (where ρ_a is the density of air, C is the wind drag coefficient, and u is wind speed). For two stronger wind episodes (10 and 8 m s^{-1}), the amounts of converted wind energy were 88 and 72 J m^{-2}. These amounts revealed a high plausibility for nutrient pulses into the upper mixed layer via wind-driven mixing in the nearshore region. For a less-saline water mass of gulf origin, on the other hand, wind energy estimates were 5–20 times less compared with the energy barrier.

A strong pycnocline due to both thermal and haline stratifications was observed on the less saline side of the front and concentrations of DIP > 0.1 μm (as clearly increased concentrations) were measured below 25–30 m (I, Fig. 5B). In the nearshore region where the along-slope jet current was observed in the intermediate layer, increased concentrations of DIP were measured at a depth of ~15 m. The stratification of the water column was also weaker, additionally diminishing the potential energy barrier. The vertical transport of phosphate into the upper layer could therefore be regarded as a two-step mechanism: shear-induced turbulence in the jet current transports nutrients from the intermediate layer to shallower depths and episodic intensive wind-induced mixing, capable of overcoming the diminished energy barrier, causes phosphate pulses into the upper mixed layer. The DIN:DIP ratio in the water below the thermocline was considerably lower than the Redfield ratio (on average, DIN:DIP was 3). Therefore, the observed initiation and development of the *Aphanizomenon* bloom was obviously supported by this gradual physical mechanism.

4.1.2. Upwelling

Two subsequent upwelling events, with a 3-weeks interval in July in the Finnish coastal sea (see Section 2.2), essentially influened the phytoplankton community and biomass (X, Table 1). Prior to and during the last upwelling there was an intensive cyanobacteria bloom in the area (40–90% of total biomass). The upwelling caused a clear decrease of the total biomass of all phytoplankton and a two-fold decrease of primary production capacity in the upper layer. The decrease of the cyanobacteria biomass was also significant, from ~120 to 20 mg ww m^{-3}. Because of different vertical distributions – *Nodularia* close to the surface and *Aphanizomenon* in the upper 15-m layer (IV, Fig. A,B; X, Fig. c,d) – almost all *Nodularia* biomass was advected offshore during the upwelling. The *Aphanizomenon* biomass decrease was less pronounced because the population residing in the thermocline was displaced upwards into the surface layer. During the upwelling (5 days), no biomass response of cyanobacteria to the high phosphate enrichment was detected, and this can be explained by temperature limitation (Lehtimäki et al., 1997).

A striking phenomenon, a significant increase in the *Aphanizomenon* biomass, was observed in two to three weeks after the initiation of both upwelling events (X, Fig. 8). The first increase was less pronounced obviously due to masking by the following upwelling event or patchiness. During the

second much stronger increase when the *Aphanizomenon* biomass reached up to 6.9 mmol C m^{-3} (comparable with main bloom biomass), the blooming in the central gulf area was already over. To verify this 'secondary' blooming of *Aphanizomenon*, its biomass increase potential during a 20-day period taking into account the observed course of surface layer temperatures (from 9.5 to 17.5 ºC) and possible losses due to sedimentation (7% d^{-1}) was estimated. Also, the bloom potential based on the measured available phosphate (0.10 mmol m^{-3}) after the relaxation of upwelling was estimated. Both estimates generally supported the observed growth of *Aphanizomenon* biomass. It is known that filamentous cyanobacteria require low phosphorus concentrations to form substantial blooms in the Baltic Sea (I). The estimates showed also that probably less than half (<0.05 mmol m^{-3}) of the available phosphate after the relaxation of upwelling was required to produce the bloom biomass. Therefore, the surplus upwelling-induced phosphate was probably involved in the uptake and recycling of other components of the phytoplankton community as well.

To summarise, single upwelling events can promote *Aphanizomenon* blooms in the coastal sea area, so even after the common summer bloom. The precondition is an about 2–3 weeks upwelling-free period prior to the bloom.

4.2. Chlorophyll patchiness

Chlorophyll *a* is a summarizing parameter of the pigment from several phytoplankton species and functional groups and therefore widely used in the plankton patchiness studies. Summer phytoplankton blooms are triggered by increasing irradiance, temperature and vertical stratification (limiting factors). The intensity of blooms depends on the availability of nutrients, grazing and sedimentation (controlling factors). The blooms are spatially heterogeneous (patchy), with a multitude of horizontal scales. The patchiness is created by the variability of physical processes and by the enhanced phytoplankton growth due to trophic enrichment and/or changes in the physiological status (Kononen and Leppänen, 1997) The physical processes modulate the phytoplankton community by the mixing of different water masses having different species composition and by the growth-stimulating effects through nutrient transport and changing illumination conditions. The chlorophyll patchiness against the background physical processes was examined by the data collected in 1996 (V, VI), when a complex of mesoscale phenomena was observed (see Sections 2.3 and 2.4).

The general development of the horizontal distribution of Chl *a* in the upper layer (within 2–6 mg Chl *a* m^{-3}) was closely related to the changing pattern of water masses with different salinity (V, cf. Fig. 2 and Fig. 3). The highest correlation between salinity and Chl *a* ($r^2 = 0.71$) was found in the region of the quasi-permanent salinity front. A Chl *a*-rich band, 5–8 km wide, was observed close to the front on its saline side (northern Baltic Proper water). A companion band with nearly the same width but with low Chl *a* concentrations was apparent on the less saline side (GOF water). The specific features, such as pronounced haline and Chl *a* cores on both sides of the front and no upwelling

indicative decrease of temperature, suggest that the along-front bandy structure of Chl *a* was caused by the differential advection of water masses from upstream areas rather than being a result of biological activity in the front (e.g. Pollard et al., 1995). After the formation of an anticyclonic eddy with saline and higher Chl *a* water in the upper layer, the less saline water with low Chl *a* was carried clockwise on its periphery. Due to the divergent flow pattern in the upper part of the eddy, the Chl *a* content in the eddy continuously decreased, so that at the final stage of observations it was lower in the eddy than in its vicinity (~60 vs. 70–90 mg Chl *a* m^{-2}). It must be added here that nutrient enrichment of the upper layer due to lifted nutricline and corresponding phytoplankton growth was frequently observed in the oceanic eddies (e.g. Hayward and Mantyla, 1990). In our case, however, the stratification was strong and therefore the wind force (2–8 m s^{-1}) was too low to cause vertical mixing at the lifted nutricline depths. Nevertheless, the possibility of a nutrient flux into the euphotic layer cannot be rejected, because the life-time of Baltic Sea eddies (one to two weeks) is long enough to create favorable preconditions.

The horizontal patchiness of Chl *a* was quantified by the coefficient of variation (CV). The mean CV over all mesoscale mappings was 18%, which is comparable with 23% obtained from the temporal series at the anchor station (VI, Table 2). Such levels of CV characterised the variability of Chl *a* due to the developing structure of water masses with different salinity and corresponding horizontal scales. At the same time the variability of species abundance was considerably high. The study period coincided with the intense blooming of *Aphanizomenon* and the dinoflagellate *Heterocapsa triquetra*, which together formed half of the total phytoplankton biomass. For *Aphanizomenon* the mean temporal and spatial variations (CV) were both about 2-fold and for *H. triquetra* 3-fold the Chl *a* variation. As no essential biological activity was observed over the study period the increased variability in the temporal species abundance must have been caused by the spatial patchiness inside the water masses carried by the current through the sampling site. Therefore it can be concluded that the horizontal scale of patches decreases and the variation of biological parameters increases when moving from the overall phytoplankton community level to the species level.

Mesoscale processes caused also noteworthy changes in the Chl *a* distribution in the vertical dimension. As a consequence of strong downwelling the chlorophyll-containing layer deepened from 15–20 to 40–45 m (V, Fig. 5), i.e. to considerably beneath the usual summer euphotic layer (10–15 m) in the western GOF. A continuous replacement by newly downwelled water may be assumed to maintain a high Chl *a* concentration at these depths. The plankton organisms were accordingly exposed to prolonged darkness for four days (duration of the downwelling event). These conditions undoubtedly affect selection, favouring those phytoplankton species that have suitable survival strategies and adaptation mechanisms for low light.

In the downwelling-associated jet the Chl *a* isopleths across the jets revealed some distinct vertical excursions (V, Fig. 6a), which are in accordance with the

expected cross-jet vertical circulation with upwelling on the anticyclonic and downwelling on the cyclonic side (Pollard and Regier, 1992). The typical undulations of the isopleths were ~10 m. The strong sinking of isopleths was caused by downward transport, resulting in significant Chl *a* concentrations (1–1.5 mg Chl *a* m^{-3}) at depths of 35–40 m. Examples of similar patterns of cross-jet chlorophyll distribution (Arnone et al., 1990; Claustre et al., 1994) and our vertical velocity estimates, definitely indicating up- and downwelling zones on the flanks of the jet (see Section 2.3), support the suggested scheme of vertical motions. The phytoplankton biomass distribution was also clearly affected by the anticyclonic eddy (V, Fig. 6b). Isopycnals above the eddy core were domed upwards, causing a corresponding lifting of the lower boundary of the Chl *a*-rich upper layer. Symmetrical signatures of the downwelled chlorophyll-containing waters were found relative to the centre of the eddy.

4.3. Subsurface chlorophyll maximum

Subsurface chlorophyll maximimum (SCM), in the oceanic literature frequently referred as deep chlorophyll maximum (DCM), is well-documented phenomenon in the seas. Usually, SCMs develop in waters where, or when, the upper layer is stratified, primary production in the surface layer is limited by the availability of nutrients, and photosyntetically active radiation penetrates into the nutrient-enriched water layer. The physical processes (e.g. fronts, eddies, near-inertial waves) can create favourable nutrient conditions in the SCM layer (Raimbault et al., 1993; Olaizola et al., 1993; Granata et al., 1995). In the Baltic Sea the SCM layers were found to be located in the seasonal thermocline, i.e. in the lower part of euphotic layer (e.g. Kahru, 1981).

A comprehensive study of the formation and development of the SCM was performed on the basis of 1994 data. The heterogeneous vertical distribution of Chl *a* during about three days gradually changed towards a relatively quasi-symmetric form (IV, Fig. 5), with decreased Chl *a* concentrations in the upper layer. This was quantitatively confirmed by the decreasing vertical stratification index, showing the degree of heterogeneity of the vertical Chl *a* distribution. In the final stage of observations the index values in the different water masses of the area approached the same level, revealing basin-wide formation of a steady SCM layer. A good positive correlation between the depth of the SCM and the density at the SCM depth (IV, Table 3) indicated that a SCM follows the vertical movement of the thermocline. A simultaneous positive correlation between the depth of the SCM and the depth of the maximum density gradient, suggested the preferred settling of the SCM onto the stability maximum of the thermocline. In several surveys, the depth and Chl *a* concentrations of the SCM were significantly negatively correlated, which certainly must reflect the increasing/decreasing availability of light for the SCM during its long-period ascents/descents with the thermocline.

The pelagial biological measurements at the fixed stations showed that the cyanobacteria bloom was in its decaying stage. Also, a marked decreasing temporal trend in the abundance of autotrophs (flagellates *Chrysocromulina*

spp. and *Ochromonas* spp. as main contributors) was observed (IV, Fig. 10, 11). This resulted in the decreasing temporal trend of Chl *a* concentration in the upper layer and therefore most likely in the formation of a SCM. However, the pelagial measurements could be considerably contaminated by the effect of physical processes. For example, in areas where the horizontal gradients of biological parameters are appreciable, the contribution of horizontal transport to local changes may become significant. To verify the contributions of physical and biochemical processes to the local changes in Chl *a* concentration (c) the property conservation equation

$$c_t = Ac_{xx} + Ac_{yy} + (Kc_z)_z - uc_x - vc_y - wc_z + c_\mathrm{b} \qquad (5)$$

was used. In Eq. 5, A is the constant horizontal eddy diffusion coefficient, K is the vertical eddy diffusion coefficient, u and v are horizontal (advective) velocity components, w is the vertical velocity component, and subscripts denote partial derivatives. The left-hand side of the equation is the local change rate of Chl *a*, while the right-hand side expresses the rate of change due to turbulent transport, advection and biochemical processes (c_b). The last term is positive when the biomass production of phytoplankton is larger than the losses (due to grazing, sinking etc.). Since biological activity is manly located in the upper layer, the mean changes over the upper 10-m layer were accounted for via vertical averaging of Eq. 5. The favourable meteorological condition (calm weather with therefore minor Ekman transport in the upper layer and vertical turbulent fluxes through the lower boundary) provided simplifications in the averaged conservation equation. The relatively low and stable currents and minimal horizontal density gradients increased the accuracy of the results. The results expressed as vertical means were comparable with the results obtained from the 'pooled' biological samples (mixture of samples taken at 1-m intervals). The used data set (towed CTD and Chl *a*, and current velocity) enabled to determine the vertically averaged Chl *a* concentration changes over 1–2 days intervals.

The most important results were the continuously negative trend of the biologically induced changes in Chl *a* and a marked contribution from the advection of Chl *a*-rich water in particular cases (IV, Table 4, Fig. 14). The calculated mean decrease in the local Chl *a* concentration due to biological processes over an one-week period was 0.18 mg Chl *a* m^{-3} d^{-1}, which is about twice the mean increase in the Chl *a* concentration (0.10 mg Chl *a* m^{-3} d^{-1}) due to physical processes. The largest physically controlled changes in the Chl *a* concentration were mainly the result of the along-gulf advection. Despite the strong cross-gulf gradient of the Chl *a* concentration, the contribution of the offshore transport of Chl *a*-rich water was small. Horizontal turbulence was also of minor importance in the formation of the Chl *a* distribution.

Thus, the development of the SCM seemed to be a pure biological process. The main biological mechanisms to be considered as loss terms, accounting for the decrease of Chl *a* in the upper layer during summer, are sedimentation and grazing. The maximum rate of Chl *a* change due to sedimentation of ca. 0.1 mg

Chl *a* m^{-3} d^{-1} was estimated, which is about half of the biological change rate of Chl *a*. The decrease of flagellates' abundance was attributed to a size-specific grazing of ciliates (continuously increasing abundances were observed in the upper layer) and was synchronously followed by reduced grazing pressure of flagellates on bacteria and picocyanobacteria. The precondition for SCM formation was the weak wind prevailing during the observations.

4.4. Deep clorophyll maximum

Deep chlorophyll maximum (DCM) layers have been frequently observed at the bottom of the euphotic layer where illumination ranges from 0.2–1% (e.g. Veldhuis and Kraay, 1990) to 10% (e.g. Mackey et al., 1995) of the surface illumination. The DCMs can be formed by species that live at low light intensity with high nutrient supply or by species that migrate vertically and acquire nutrients at depth, where light limits growth rate (Cullen and MacInture, 1998). As a rare occurrence, DCMs have been observed in darkness well below the level of illumination where photosynthesis can occur, i.e., at illumination <0.1% of the sea surface (Washburn et al., 1991). In the Baltic Sea the chlorophyll maxima well beneath the euphotic layer were first observed in our study area during experiments in 1996 and 1998 (V, VII).

As the Baltic Sea is relatively turbid, the mean depth corresponding to 0.1% surface light intensity is about 15 m. In 1996, 894 (7 mesoscale mappings) DCM layers were recorded in the depth range 30–50 m. The DCM layers were commonly 0.5–2 m thick and 75% of peak Chl *a* concentrations were in the range 1.5–3 mg Chl *a* m^{-3} with a maximum value of 24.8 mg Chl *a* m^{-3}. In 1998, 589 (5 mappings) observed SCM layers had a mean thickness of 5–6 m and the mean depth increased from 30 m to 35 m by the end of the study (VII, Table 2). The mean peak Chl *a* concentrations were mostly <2 mg Chl *a* m^{-3}, while the highest value was 10.1 mg Chl *a* m^{-3}. The mean amount of Chl *a* in the DCM layer formed 6–10% of the mean chlorophyll content in the water column above 25 m depth. The deeper location and smaller thickness of the DCM in 1996 could be explained by the influence of mesoscale phenomena (downwelling, anticyclonic eddy and related jets) causing significant vertical movements of isopycnal surfaces from 30–35 m to about 50 m and also a squeezing of isopycnals (see Section 2.4).

In both years the exceptionally cold and windy weather led to a bloom of a motile, nitrate-sensitive dinoflagellate *Heterocapsa triquetra* in the upper layer. The DCM layers were clearly dominated by *H. triquetra* and located in the top of the nitracline. There are two possible mechanisms that can cause DCM – it may result from the advective transport of water masses or be created by vertically migrating *H. triquetra* cells as a response to the changing environmental conditions due to physical processes. Both aspects were evaluated using physical and biological measurements in 1998. The former one was rejected because the DCM appeared in the relatively cold (4–5 ºC) water mass (VII, Table 2) flowing out of the GOF along the Finnish coast, and thus was not caused by the flow of water masses from the euphotic layer along

sloping isopycnal surfaces. Also, the cold and phosphate-rich intrusions likely spreading from inshore regions contained no maxima on fluorescence profiles (VII, Fig. 8). The DCM layers were situated deeper than intrusions and had a higher density, and therefore were not related to the intrusive layering.

The DCM appeared after a strong SW wind event, which caused upwelling and stimulated wind-induced turbulence. The surplus phosphate and therefore shortage of nitrogen for *H. triquetra* cells in the upper layer after the upwelling event obviously changed the diel migratory behaviour of cells. So, instead of returning to the surface layer they continued moving downward, i.e. towards the deeper nitrogen reserve. Turbulent mixing might have three roles in the formation and maintenance of the DCM.

First, it may create and maintain small gradients of nitrate in the water column above the deep nitracline, which guides the swimming direction of nitrogen-starved cells (chemotactical response). Integration of the simplified diffusion equation (Eq. 4) for 1 day, using the measured eddy coefficient and vertical nitrate profiles, indicates that turbulence could have resulted in nitrate concentrations of $1–3 \times 10^{-4}$ mmol m^{-3} to a depth of about 20 m. If we assume that the diel migration was ca. 10 m, the *H. triquetra* cells could therefore have sensed the nitrate concentration gradient during a diel migratory cycle.

Secondly, turbulent mixing may support the downward migration of *H. triquetra* cells from the bottom of the euphotic layer. Calculation based on measured eddy coefficient and Chl *a* profiles gave negative Chl *a* fluxes up to 1.5 mg Chl *a* m^{-2} d^{-1} in the bottom of the chlorophyll-containing layer (VII, Fig. 10c), which clearly indicates downward mixing of Chl *a* and consequently cells of *H. triquetra*.

Thirdly, turbulent mixing may move cells out of the top of the nitracline and therefore destroy the DCM. To estimate the swimming speed (w) necessary to maintain the DCM, the relationship $w = K\,\partial \ln n_s/\partial z$ was used (Lande et al., 1989), where n_s is the species abundance. Considering the largest change of *H. triquetra* abundance of $\sim 1.2 \times 10^6$ cell l^{-1} along 1.7 m and typical eddy coefficient (2×10^{-5} m^2 s^{-1}) in the DCM layer, w is ~0.1 m h^{-1}. That is much less than the migration speed of *H. triquetra* of about 1 m h^{-1}, i.e. the migration speed of *H. triquetra* was sufficient to maintain the DCM.

Thus, physical processes support the formation of the DCM by changing environmental conditions (input of phosphate into the upper layer, creation of small nitrate gradients above the nitracline) and by transporting *H. triquetra* cells downward out from the chlorophyll-containing layer.

CONCLUSIONS

The case studies of mesoscale physical phenomena enabled to determine their spatial structure and temporal development.

- The quasi-permanent salinity front at the entrance to the GOF is highly sensitive to the wind direction. Easterly winds (parallel to the front) cause offshore movement of denser water, as well as a stronger inclination of the front to the sea surface. With westerly winds, the less dense water moves onshore and overrides the denser water, thus forming a shallower secondary pycnocline. Wind-induced changes in the frontal zone structure are well described by a semi-empirical model.
- Single upwelling events and associated filaments at the Finnish coast had remarkable signatures of colder water about three weeks after the relaxation of the wind. The filaments extended to the central GOF and were almost at the same locations in different years, which refers to the instability of the upwelling front due to features of bottom topography and/or coastline.
- A downwelling-related meandering jet current transformed into an anticyclonic eddy with a strong jet-like current in its periphery. The cyclonic and anticyclonic relative vorticity bands induced by these processes had comparable maximum values of $\sim f$. The maximum vertical up- and downward velocities (estimated by the quasi-geostrophic ω-equation diagnostic technique) in the downwelling jet were 35 and 26 m d^{-1}, respectively.

Seasonal nutriclines have a firm vertical ordering: silicocline, phosphacline and nitracline. The seasonal dynamics of phytoplankton biomass and species composition together with nutrient conditions (inter-annual changes in external and internal loads) probably determine the depth and separation of seasonal phosphacline and nitracline. Mesoscale physical processes cause mainly reversible displacements and intrusive layering of nutriclines.

Physical processes are important in the initiation of cyanobacteria blooms. The formation of a *Nodularia spumigena* bloom started in the shallow sub-surface mixed layer, which formed due to differential advection of water masses in the frontal zone. A bloom of *Aphanizomenon flos-aquae* was initiated by the vertical phosphate pulses into the upper layer via the gradual physical mechanism (shear-induced turbulence in the front-related jet current overlaid by episodic intensive wind-induced mixing). In the coastal sea area the growth of *Aphanizomenon* was promoted by the phosphate input during the upwelling events with a 2–3 weeks lag.

Mesoscale physical processes considerably modulate the horizontal distribution of chlorophyll i.e. create continuously changing patchy structure. Vertical movements of chlorophyll-rich water are addressed to the downwelling and vertical circulation patterns in jets and anticyclonic eddy.

The deep chlorophyll maximum was not caused by intrusions from neighbouring areas. It formed as a result of changing migratory behaviour of the

dinoflagellate *Heterocapsa triquetra* after an upwelling event (changed nutrient conditions), which was supported by the turbulent mixing (enhancing upward nitrate fluxes and downward transport of cells).

The formation of the subsurface chlorophyll maximum is a purely biological process, which was confirmed by the estimates via a three-dimentional property (chlorophyll) conservation equation and pelagial measurements.

ACKNOWLEDGEMENTS

The findings presented in this thesis are a result of collective work carried out mainly by a small group of scientists from the Finnish Institute of Marine Research and Marine Systems Institute at TUT. Therefore, I wish to express my deepest gratitude to all of them. Especially, I want to thank Dr. Kaisa Kononen who initiated the multidisciplinary joint investigations and with a great enthusiasm led us during all these years. I also want to thank her for introducing me to the world of marine biology and for thoroughness and patience in endless but very fruitful discussions.

I am grateful to Dr. Jaan Laanemets, a good colleague and friend over more than thirty years, for his help and advice in supervising my thesis. I also wish to express my gratitude to all the people of my generation in the Marine Systems Institute for motivating me to be at last graduated. I thank all of them for being good companions in the field of marine sciences and for a pleasant time spent together. I am also grateful to Ants Pastarus and Henry Söderman for the technical support during all cruises, which enabled to collect a unique physical data set.

I also wish to express my warmest thanks to Prof. Ain Aitsam, restorer of the studies of marine physics in Estonia and my first teacher, who guided me into the field of science and taught me more than just science.

I want to thank the Maj and Tor Nessling Foundation (Finland) for the financial support in 1993–2002, which made it possible to perform the majority of studies presented in this thesis. The Estonian Science Foundation (Grant No. 2195) is also acknowledged.

Finally, I want to thank my family for the understanding and for tolerant attitude to my profession and long periods of absence from home due to the work.

REFERENCES

Aitsam, A. and Elken, J. (1982). Synoptic scale variability of hydrophysical fields in the Baltic Proper on the basis of CTD measurements. *In*: Hydrodynamics of semi-enclosed seas. J. C. J. Nihoul (editor). Elsevier, Amsterdam, 433–467.

Aitsam, A. and Talpsepp, L. (1982). Synoptic variability of currents in the Baltic Proper. *In*: Hydrodynamics of Semi-enclosed Seas. J. C. J. Nihoul (editor). Elsevier, Amsterdam, 469–488.

Aitsam, A., Hansen, H. P., Elken, J., Kahru, M., Laanemets, J., Pajuste, M., Pavelson, J. and Talpsepp, L. (1984). Physical and chemical variability of the Baltic Sea: a joint experiment in the Gotland Basin. – Continental Shelf Research, 3, 291–310.

Alenius, P., Myrberg, K. and Nekrassov, A. (1998). Physical oceanography of the Gulf of Finland: a review. – Boreal Environment Research, 3, 97–125.

Alenius, P., Nekrasov, A. and Myrberg, K. (2003). Variability of the baroclinic Rossby radius in the Gulf of Finland. – Continental Shelf Research, 23, 563–573.

Allen, J. S. and Newberger, P. A. (1996). Downwelling circulation on the Oregon continental shelf, Part I: response to idealized forcing. – Journal of Physical Oceanography, 26, 2011–2035.

Allen, J. T. and Smeed, D. A. (1996). Potential vorticity and vertical velocity at the Iceland-Færœs front. – Journal of Physical Oceanography, 26, 2611–2634.

Andrejev, O., Myrberg, K., Alenius, P. and Lundberg, A. (2004). Mean circulation and water exchange in the Gulf of Finland – a study based on three-dimensional modeling. – Boreal Environment Research, 9, 1–16.

Armi, L., Herbert, D., Oakey, N., Price, J., Richardson, P., Rossby, T. and Ruddick, B. (1989). Two years in the life of a Mediterranean salt lens. – Journal of Physical Oceanography, 19, 354–370.

Arnone, R. A., Wiesenburg, D. A. and Saunders, K. D. (1990). The origin and characteristics of the Algerian Current. – Journal of Geophysical Research, 95, 1587–1598.

Blanton J. O., Oey, L.-Y., Amft, J. and Lee, T. N. (1989). Advection of momentum and buoyancy in a coastal frontal zone. – Journal of Physical Oceanography, 19, 98–115.

Carbonel, C. A. A. H. (2003). Modelling of upwelling–downwelling cycles caused by variable wind in a very sensitive coastal system. – Continental Shelf Research, 23, 1559–1578.

Claustre, H., Kerhervé, P., Marty, J. C., Prieur, L., Videau, C. and Hecq, J.-H. (1994). Phytoplankton dynamics associated with a geostrophic front: ecological and biological implications. – Journal of Marine Research, 52, 711–742.

Cullen, J. J. and MacIntyre, J. G. (1998). Behaviour, physiology and niche of depth-regulating phytoplankton. *In*: NATO ASI Series Vol. G41. Physiological ecology of phytoplankton. D. M. Anderson, A. D. Cembella and G. M. Hallegraeff (editors), Springer-Verlag, 559–579.

Elken, J., Talpsepp, L., Kõuts, T. and Pajuste, M. (1994). The role of mesoscale eddies and saline stratification in the generation of spring bloom heterogeneity in the southeastern Gotland Basin: an example from PEX ’86. – ICES Cooperative Research Report, 201, 40–48.

Elken, J. (1994). Numerical study of fronts between the Baltic sub-basins. *In*: Proceedings of the 19th Conference of the Baltic Oceanographers. Sopot, Poland, 438–446.

Elken, J. (1996). Deep water overflow, circulation and vertical exchange in the Baltic Proper. Estonian Marine Institute Report Series, 6. 91 pp.

Elken, J., Raudsepp, U. and Lips, U. (2003). On the estuarine transport reversal in deep layers of the Gulf of Finland. – Journal of Sea Research, 49, 267–274.

Fedorov, K. N. (1986). The physical nature and structure of oceanic fronts. Springer-Verlag. 333 pp.

Feliks, Y. (1991). Downwelling along the northeastern coasts of the Eastern Mediterranean. – Journal of Physical Oceanography, 21, 511–526.

Feliks, Y. and Ghil, M. (1993). Downwelling-front instability and eddy formation in the Eastern Mediterranean. – Journal of Physical Oceanography, 23, 61–78.

Fennel, W., Seifert, T. and Kayser, B. (1991). Rossby radii and phase speeds in the Baltic Sea. – Continental Shelf Research, 11, 23–36.

Fonselius, S. and Valderrama, J. (1994). Some results from the participation of 'Argos' in PEX '86. – ICES Cooperative Research Report, 201, 49–59.

Granata, T., Wiggert, J. and Dickey, T. (1995). Trapped, near-inertial waves and enhanced chlorophyll distributions. – Journal of Geophysical Research, 100, 19793–20804.

Granéli, E., Wallström, K., Larsson, U., Granéli, W. and Elmgren, R. (1990). Nutrient limitation of primary production in the Baltic Sea area. – Ambio, 19, 142–151.

Haapala, J. (1994). Upwelling and its influence on nutrient concentration in the coastal area of the Hanko Peninsula, entrance to the Gulf of Finland. – Estuarine, Coastal and Shelf Science, 38, 507–521.

Hayward, T. L. and Mantyla, A. W. (1990). Physical, chemical and biological structure of a coastal eddy near Cape Mendocino. – Journal of Marine Research, 48, 825–850.

HELCOM (1990). Second periodic assessment of the state of the marine environment of the Baltic Sea, 1984–1988; Background Document. – Baltic Sea Environment Proceedings, 35B.

HELCOM (2002). Environment of the Baltic Sea area 1994–1998. – Baltic Sea Environment Proceedings, 82B.

Hoskins, B. J., Draghici, I. and Davies, H. C. (1978). A new look at the ω-equation. – Quarterly Journal of Royal Meteorology Society, 104, 31–38.

Huthnance, J. M. (1995). Circulation, exchange and water masses at the ocean margin: the role of physical processes at the shelf edge. – Progress in Oceanography, 35, 353–431.

Kahru, M. (1981). Relations between the depths of chlorophyll maxima and the vertical structure of the density field in the Baltic Sea. – Oceanology, 21, 76–79.

Kahru, M., Håkansson, B. and Rud, O. (1995). Distributions of the sea-surface temperature fronts in the Baltic Sea as derived from satellite imagery. – Continental Shelf Research, 15, 663–679.

Kahru, M., Leppänen, J.-M., Rud, O. and Savchuk, O. P. (2000). Cyanobacteria blooms in the Gulf of Finland triggered by saltwater inflow into the Baltic Sea. – Marine Ecology Progress Series, 207, 13–18.

Kamenkovich, V. M., M. N. Koshlyakov, M. N. and Monin, A. S. (1986). Synoptic eddies in the ocean. D. Reidel Publishing Company. 433 pp.

Kanoshina, I., Lips, U. and Leppänen, J.-M. (2003). The influence of weather conditions (temperature and wind) on cyanobacterial bloom development in the Gulf of Finland. – Harmful Algae, 2, 29–41.

Kivi, K., Kaitala, S., Kuosa, H., Kuparinen, J., Leskinen, E., Lignell, R., Marcussen, B. and Tamminen, T. (1993). Nutrient limitation and grazing control of Baltic plankton community during annual succession. – Limnology and Oceanography, 38, 893–905.

Kononen, K. (1992). Dynamics of the toxic cyanobacterial blooms in the Baltic Sea. – Finnish Marine Research, 261, 1–36.

Kononen, K. and Nõmmann, S. (1992). Spatio-temporal dynamics of the cyanobacterial blooms in the Gulf of Finland, Baltic Sea. *In*: Marine Pelagic Cyanobacteria: Trichodesmium and Other Diazotrophs. E. J. Carpenter, D. Capone and J. Rueter (editors), Kluwer, Dordrecht, 95–113.

Kononen, K. and Leppänen, J.-M. (1997). Patchiness, scales and controlling mechanisms of cyanobacterial blooms in the Baltic Sea: application of a multi-scale researc strategy. *In*: Monitoring Algal Blooms: New Techniques for Detecting Large-Scale Environmental Change. M. Kahru and Ch. W. Brown (editors), Landes Bioscience, Austin, TX, USA, 63–84.

Laamanen, M. and Kuosa, H. (2005). Annual variability of biomass and heterocysts of N_2-fixing cyanobacterium *Aphanizomenon floa-aquae* in the Baltic Sea with reference to *Anabena* spp. and *Nodularia spumigena*. – Boreal Environment Research, 10, 19–30.

Lande, R., Li, W. K. W., Hornet, E. P. W. and Wood, A. M. (1989). Phytoplankton growth rates estimated from the depth profiles of cell concentration and turbulent diffusion. – Deep-Sea Research, 36, 1141–1159.

Larsson, U., Hajdu, S., Walve, J. and Elmgren, R. (2001). Baltic Sea nitrogen fixation estimated from the summer increase in upper mixed layer total nitrogen. – Limnology and Oceanography, 46, 811–820.

Leach, H. (1987). The diagnosis of synoptic-scale vertical motion in the seasonal thermocline. – Deep-Sea Research, 34, 2005–2017.

Lehmann, A. (1995). A three-dimensional baroclinic eddy-resolving model of the Baltic Sea. – Tellus, A47, 1013–1031.

Lehtimäki, J., Moisander, P., Sivonen, K. and Kononen, K. (1997). Growth, nitrogen fixation, and nodularin production by two Baltic Sea cyanobacteria. – Applied and Environmental Microbiology, 63, 1647–1656.

Lignell, R., Seppälä, J., Kuuppo, P., Tamminen, T., Andersen, T. and Gismervik, I. (2003). Beyond bulk properties: responses of coastal summer plankton communities to nutrient enrichment in the northern Baltic Sea. – Limnology and Oceanography, 48, 189–209.

Lilover, M.-J., Laanemets, J., Kullas, T., Stips, A. and Kononen, K. (2003). Late summer vertical nutrient fluxes estimated from direct turbulence measurements: Gulf of Finland case study. – Proceedings of the Estonian Academy of Science. Biology. Ecolology, 53, 193–204.

Lundberg, L. and Rydberg, L. (1994). Calculation of vertical heat transfer, nutrient uptake, and oxygen production during the Baltic Sea spring bloom in 1986. – ICES Cooperative Research Reports, 201, 73–84.

Mackey, D. J., Parslow, J., Higgins, H. W., Griffith, F. B. and O'Sullivan, J.E. (1995). Plankton productivity and biomass in the western equatorial Pacific: biologial and physical controls. – Deep-Sea Research, 42, 499–533.

Mann, K. H. and Lazier, J. R. N. (1991). Dynamics of marine ecosystems. Blackwell, Boston, MA. 466 pp.

Monin, A. S., Kamenkovich, V. M. and Kort, V. G. (1977). Variability of the oceans. John Wiley and Sons. 241 pp.

Myrberg, K. and Andrejev, O. (2003). Main upwelling regions in the Baltic Sea – a statistical analysis based on three-dimensional modelling. – Boreal Environment Research, 8, 97–112.

Niemi, Å. (1979). Blue-green algal blooms and N:P ratio in the Baltic Sea. – Acta Botanica Fennica, 110, 57–61.

Oey, L.-Y., Atkinson, L. P. and Blanton, J. O. (1987). Shoreward intrusion of upper Gulf Stream water onto the U.S. southeastern continental shelf. – Journal of Physical Oceanography, 17, 2318–2333.

Olaizola, M., Ziemann, D. A., Bienfang, P. K., Walsh, W. A. and Conquest, L. D. (1993). Eddy-induced oscillations of the pycnocline affect the floristic composition and depth distribution of phytoplankton in the Subtropical Pacific. – Marine Biology, 116, 533–542.

Onken, R. (1992). Mesoscale upwelling and density finestructure in the seasonal thermocline – a dynamical model. – Journal of Physical Oceanography, 22, 1257–1273.

Pavelson, J. (1988). Nature and some characteristics of thermohaline fronts in the Baltic Proper. *In*: Proceedings of the 16th Conference of the Baltic Oceanographers, Kiel, Germany, 796–805.

Peliz, Á., Rosa, T. L., Santos, A. M. and Pissarra, J. L. (2002). Fronts, jets, and counter flows in the Western Iberian upwelling system. – Journal of Marine Systems, 35, 61–77.

Pingree, R. D. and Le Cann, B. (1992). Three anticyclonic Slope Water Oceanic eDDIES (SWODDIES) in the Southern Bay of Biscay in 1990. – Deep-Sea Research, 39, 1147–1175.

Pinot, J.-M., Tintoré, J. and Wang, D.-P. (1996). A study of the omega equation for diagnosing vertical motion at ocean fronts. – Journal of Marine Research, 54, 239–259.

Pitkänen, H., Lehtoranta, J. and Räike, A. (2001). Internal nutrient fluxes counteract decreases in external load: the case of the estuarial eastern Gulf of Finland, Baltic Sea. – Ambio, 30, 195–201.

Pollard, R. T. and Regier, L. (1990). Large variations in potential vorticity at small spatial scales in the upper ocean. – Nature, 348, 227–229.

Pollard, R. T. and Regier, L. A. (1992). Vorticity and vertical circulation at an ocean front. – Journal of Physical Oceanography, 22, 609–625.

Pollard, R. T., Read, J. F., Allen, J. T., Griffiths, G., and Morrison, A. I. (1995). On the physical structure of a front in the Bellingshausen Sea. – Deep-Sea Research, 42: 955–982.

Rahm, L., Jönsson, A. and Wulff, F. (2000). Nitrogen fixation in the Baltic proper: an empirical study. – Journal of Marine Systems, 25, 239–248.

Raimbault, P., Coste, B., Boulhadid, M. and Boudjellal, B. (1993). Origin of high phytoplankton concentration in deep chlorophyll maximum (DCM) in a frontal region of the Southwestern Mediterranean Sea. – Deep-Sea Research, 40, 791–804.

Shearman, R. K., Barth, J. A. and Kosro P. M. (1999). Diagnosis of the three-dimensional circulation associated with mesoscale motion in the California Current. – Journal of Physical Oceanography, 29, 651–670.

Soomere, T. and Keevallik, S. (2003). Directional and extreme wind properties in the Gulf of Finland. – Proceedings of the Estonian Academy of Science. Engineering, 9, 73–90.

Stigebrandt, A., Lass, H.-U., Liljebladh, B., Alenius, P., Piechura, J., Hietala, R. and Beszczyńska, A. (2002). DIAMIX – an experimental study of diapycnal deepwater mixing in the virtually tideless Baltic Sea. – Boreal Environment Research, 7, 363–369.

Stipa, T. (2004). Baroclinic adjustment in the Finnish coastal current. – Tellus, 56A, 79–87.

Stommel, H. and Fedorov, K. N. (1967). Small-scale structure in temperature and salinity near Timor and Mindanoa. – Tellus, 19, 76–81.

Strub, P. T., Kosro, P. M. and Huyer, A. (1991). The nature of the cold filaments in the California Current system. – Journal of Geophysical Research, C96, 14743–14768.

Talpsepp, L. (1993). Investigations of mesoscale hydrophysical processes in the Gulf of Finland in 1985–1990. – Proceedings of the Estonian Academy of Sciences. Ecology, 3, 137–148.

Talpsepp, L., Nõges, T., Raid, T. and Kõuts, T. (1994). Hydrophysical and hydrobiological processes in the Gulf of Finland in summer 1987: characterization and relationship. – Continental Shelf Research, 14, 749–763.

Veldhuis, M. J. C. and Kraay, G. W. (1990). Vertical distribution and pigment composition of a picoplanktonic prochlorophyte in the subtropical North Atlantic: a combined study of HPLC-analysis of pigments and flow cytometry. – Marine Ecology Progress Series, 68, 121–127.

Washburn, L., Kadko, D. C., Jones, B. H., Hayward, T., Kosro, P. M., Stanton, T. P., Ramp, S. and Cowles, T. (1991). Water mass subduction and the transport of phytoplankton in a coastal upwelling system. – Journal of Geophysical Research, C96, 14927–14945.

Wasmund, N. (1997). Occurrence of cyanobacterial blooms in the Baltic Sea in relation to environmental conditions. – Hydrobiologia, 82, 169–184.

Zhurbas, V., Stipa, T., Mälkki, P., Paka, V., Golenko, N., Hense, I. and Sklyarov, V. (2004). Generation of subsurface cyclonic eddies in the southeast Baltic Sea: Observations and numerical experiments. – Journal of Geophysical Research, 109, C05033, doi: 10.1029/2003JC002074.